Numerical Study of Laser-Sustained Hydrogen Plasmas in a Forced Convective Flow

San-Mou Jeng* and Dennis R. Keefer†
The University of Tennessee Space Institute, Tullahoma, Tennessee

A two-dimensional numerical model for laser-sustained argon plasmas, which considers laminar Navier-Stokes equations and real ray tracing for the laser beam, has been extended for forced convective hydrogen plasmas. Realistic thermodynamic, transport, and optical properties of hydrogen were incorporated into the calculations. Parametric studies of inlet gas velocity, static pressure, laser power, and laser beam diameter have been conducted. Calculated plasma size, temperature distribution, flowfield, and energy conversion efficiency are presented in this paper. It was found that the constant axial mass flux (product of axial velocity and density) assumption which has been used in one-dimensional and quasi-two-dimensional models is not adequate for this problem. The results also revealed that plasma size, position, and radiation heat loss can be controlled by varying optical arrangements and operating conditions.

Nomenclature

c_p = specific heat at constant pressure, J/kg-K
I_i = laser intensity of each ray, W/m^2
k = intrinsic thermal conductivity, W/m-K
k_{eff} = effective thermal conductivity, W/m-K
k_{rad} = radiation-induced thermal conductivity, W/m-K
h = specific enthalpy, J/kg
$\dot{q}_{\text{rad}}$ = radiation heat loss, J/m^3-s
r = radius, m
s = distance along the laser ray, m
T = temperature, K
u = axial velocity, m/s
v = radial velocity, m/s
x = axial distance, m
y = radial distance, m
α = absorption coefficient at 10.6 μm wavelength, 1/m
μ = viscosity, kg/m-s
ρ = density, kg/m^2

Introduction

SINCE the laser thermal propulsion concept was first proposed,[1] many investigations have evaluated this concept. Either pulsed or continuous-wave laser-power thrusters have been suggested, and most investigations are still limited to the fundamental understanding of the problem. One of the most promising approaches is to use the laser-sustained plasma (LSP) to absorb laser energy into the propellant. The major advantages of the laser thruster for a propulsion system, as compared to a conventional chemical propulsion rocket, are that the lowest possible molecular-weight propellant (pure hydrogen) can be used, and that the maximum temperature, which is related to the specific impulse of a propulsion device, is not limited to the flame temperature of a combustion process. In addition, the laser is located remotely, and the space vehicle does not need to carry heavy onboard equipment, so the payload can be increased.

Received April 11, 1986; presented as Paper 86-1524 at the AIAA/ASME/SAE/ASEE Joint Propulsion Conference, Huntsville, AL, June 16-18, 1986; revision received Sept. 8, 1986.

*Senior Engineer, The Center for Laser Applications. Member AIAA.
†Professor, Engineering Science & Mechanics, The Center for Laser Applications. Member AIAA.

Hydrogen is transparent to laser irradiation at low temperature, and one way to convert laser energy to heat in flowing hydrogen is to have a part of the working fluid in an ionized plasma state that absorbs laser energy very effectively. Figure 1 shows a sketch for a proposed laser thermal propulsion thruster. Hydrogen propellant enters the absorption chamber through the annular slot near the inner surface of the lens. The laser beam from the remote site is focused into the chamber. Laser energy is absorbed and sustains a high-temperature hydrogen plasma core, heating the flow that is accelerated through the nozzle to produce the required thrust. In a practical laser thruster, the interaction between the laser beam and plasma occurs near the centerline of the absorption chamber, so the cold, unheated layer of flow near the wall keeps the wall from melting. In addition to the convective energy transferred to the wall, thermal radiation from the plasma contributes to wall heating and also reduces the efficiency of thermal conversion from laser energy to the flow enthalpy. Thus, a basic understanding of the properties of LSP is needed before designing a laser propulsion thruster.

Since an LSP has highly nonlinear thermodynamic transport and optical properties, and extremely high absorption of laser energy by the flow, a solution to this problem is not easily achieved. Several one-dimensional and quasi-two-dimensional models of LSP have been reported.[2-8] Merkle and co-workers[9-12] recently used a contemporary numerical method to attack the full two-dimensional problem. They succeeded in the calculation of a low-temperature LSP (peak temperature about 4000 K) in a hydrogen flow seeded with cesium. It is feasible to extend their approach to a pure hydrogen plasma, but the higher peak temperature (about 16,000 K) and much stronger nonlinear optical properties of the pure hydrogen plasma can result in numerical stability problems.

Recently Jeng and Keefer[13] obtained a numerical solution for a rigorous two-dimensional model with realistic gas properties for the LSP in an argon flow. Their results agreed well with experimental data[14,15] in plasma position, size, shape, and peak temperature. Jeng and Keefer[16] have also studied the effect of laser power, flow rate, static pressure, and optics on the argon LSP. The predicted properties of the argon LSP at different conditions followed the trends experimentally observed by Welle et al.[17] Their work also indicated that there are no fatal errors in the laser propulsion concept, and the critical parameters, for example, plasma size, position, radiation heat loss, and energy conversion efficiency, can be con-

trolled using an appropriate optical arrangement and a suitable flow configuration.

In this study, a two-dimensional model was extended to predict the properties of an LSP in a hydrogen flow. The model is similar to the early version[13,16] for an argon LSP. The major features of the model are: the use of two-dimensional flow and energy equations; the use of more realistic hydrogen gas properties, which include radiation emission and absorption coefficients, transport and thermodynamic properties; and the use of geometric optics to trace the laser beam through the focusing system. The objectives of this investigation are to understand the physical processes of the LSP, to estimate the hydrogen LSP properties, and to predict the energy conversion efficiency under different test conditions. In order to achieve these goals, calculations using different inlet velocity, pressure, laser power, and laser beam size were performed.

Theoretical Model

Ideally, the model would simulate the flow geometry shown in Fig. 1. However, in order to gain more understanding of the interactions between laser and plasma, the simple flow geometry as shown in Fig. 2. was adopted. It is assumed that this domain is axisymmetric, and a cylindrical coordinate system was employed. The incoming working fluid enters from the bottom, and the originally collimated 10.6-μm carbon dioxide laser beam is focused into the gas by an appropriate lens.

It was assumed that the flow is laminar, steady-state, and axisymmetric, and has variable physical properties. The pressure of the flow is relatively high, so that local thermodynamic equilibrium (LTE) can be assumed with little error. Therefore, the plasma can be described by a single temperature, and its physical properties are only a function of this temperature and pressure. Thermal radiation was divided into two parts: an optically thin portion in which all radiation escapes from the plasma, and an optically thick portion that can be described as a diffusion process. Since the Mach number for the flow is small, the kinetic energy and viscous dissipation were neglected in the energy equation. Following the above assumptions and using the viscous terms of incompressible flow, which have been discussed in the previous study,[13] the equations of conservation of mass, momentum, and energy for the flow can be written

$$\frac{\partial(\rho u)}{\partial x}+\frac{1}{r}\frac{\partial(r\rho v)}{\partial r}=0 \tag{1}$$

$$\frac{\partial(\rho uu)}{\partial x}+\frac{1}{r}\frac{\partial(r\rho uv)}{\partial r}=-\frac{\partial p}{\partial x}-\rho g+\left[\frac{\partial}{\partial x}\left(\mu\frac{\partial u}{\partial x}\right)+\frac{1}{r}\frac{\partial}{\partial r}\left(\mu r\frac{\partial u}{\partial r}\right)\right] \tag{2}$$

$$\frac{\partial(\rho uv)}{\partial x}+\frac{1}{r}\frac{\partial(r\rho vv)}{\partial r}=-\frac{\partial p}{\partial r}+\left[\frac{\partial}{\partial x}\left(\mu\frac{\partial v}{\partial x}\right)+\frac{1}{r}\frac{\partial}{\partial r}\left(\mu r\frac{\partial v}{\partial r}\right)\right]-\frac{2\mu v}{r^2} \tag{3}$$

$$\frac{\partial(\rho uh)}{\partial x}+\frac{1}{r}\frac{\partial(\rho rvh)}{\partial r}=\frac{\partial}{\partial x}\left[\frac{k_{\text{eff}}}{c_p}\frac{\partial h}{\partial x}\right]+\frac{1}{r}\frac{\partial}{\partial r}\left[\frac{rk_{\text{eff}}}{c_p}\frac{\partial h}{\partial r}\right]+\Sigma\alpha I_i-\dot{q}_{\text{rad}} \tag{4}$$

where I_i is the local intensity of each laser ray, which is described by the following equation

$$\frac{dI_i}{ds}=-\alpha I_i \tag{5}$$

and s is the distance along the laser propagation direction. The laser beam path through the optical system was calculated by geometric ray tracing. Diffraction of the laser beam due to the finite aperture of the lens and effects due to the inhomogeneous refractive index within the plasma were neglected in the calculation, since Welle et al.[17] had found that these assumptions produced little error on the calculated results.

Gas Properties

The thermodynamic properties (density, enthalpy, and specific heat) were found and linearly interpolated from the tabulated values of Patch,[18] whose model considered spin-equilibrated hydrogen in chemical equilibrium in the Debye-Huckel approximation. The magnitude of the specific heat of hydrogen is much higher than that of argon; in addition, hydrogen needs a large amount of energy for dissociation, so the observed maintenance threshold laser power for hydrogen plasmas is much larger than that of argon plasmas.[19]

The intrinsic transport properties (thermal conductivity and viscosity) at temperatures below 8000 K were found and interpolated from tabulated values of Grier,[20] whose analysis neglected the effect of ionization; at higher temperatures, tabulated values from Ref. 21 were used. The expression for

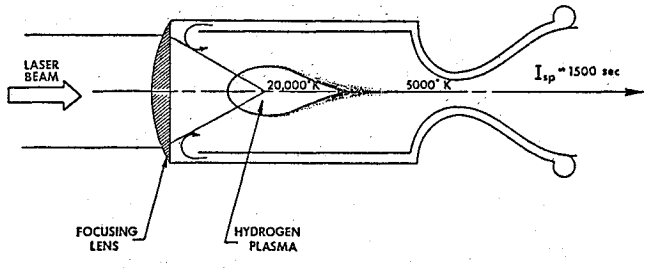

Fig. 1 Schematic configuration for a laser absorption chamber.

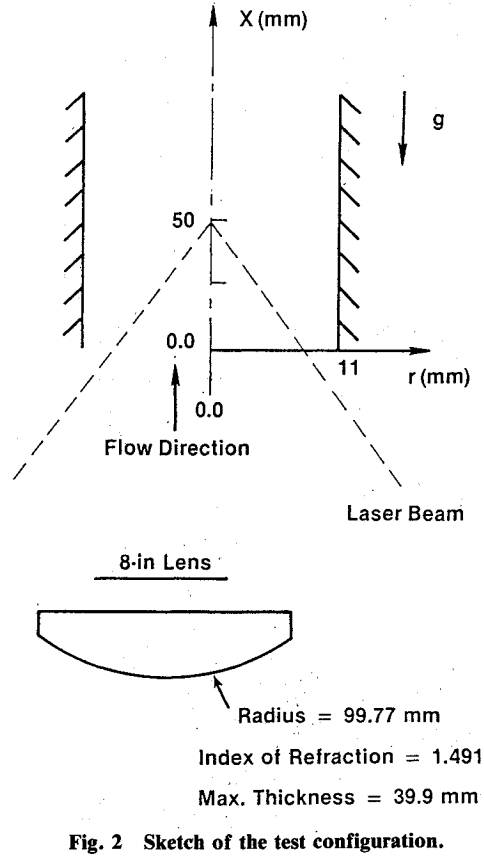

Fig. 2 Sketch of the test configuration.

radiation-induced thermal conductivity is not trivial; it is not a gas property, and it depends on the actual size and radiation characteristics of the plasma. Kemp and Root[22,23] found that the radiation can be approximated as optically thick at wavelengths less than 0.095 μm. Their theoretically derived expression for radiation-induced thermal conductivity was adopted in the current study. At temperatures below 10,000 K, the radiation-induced thermal conductivity is very small compared to the intrinsic thermal conductivity. The radiation thermal conductivity increases very rapidly as the temperature increases from 10,000 K. At 15,000 K, its magnitude is about three orders higher than that of the intrinsic thermal conductivity.

The expression for the absorption coefficient at 10.6 μm was adopted from Caledonia et al.[24] They considered both electron-ion and electron-neutral inverse bremsstrahlung. Hydrogen at temperatures below 10,000 K is transparent to the laser irradiation because of its very low electron density. As temperature increases from 10,000 K, ionization of the plasma increases, and the absorption coefficient also increases. Around 16,000–20,000 K, the plasma is almost fully ionized, and the absorption reaches a maximum because the total density decreases with further increases in temperature. As the pressure increases, the maximum absorption coefficient also increases, and its pressure dependence is approximately $p^{1.5}$.

Radiation heat loss from the plasma includes both line and continuum contributions at wavelengths larger than 0.095 μm. The expression analytically derived by Kemp et al.[25] was adopted. The pressure dependence of radiation heat loss is similar to the absorption coefficient and is approximately proportional to $p^{1.5}$.

Finite-Difference Solution

The finite-difference solution procedure employed in this work is an adaptation of the method described in detail by Patankar.[26] Detailed description of the numerical procedure used in the current calculation was discussed in Jeng and Keefer,[13] and only a brief description is presented in this section. The SIMPLE[26,27] algorithm, which uses a conservative form of the finite-difference equation, primitive variables, and staggered grids, was adopted to solve the coupled mass, momentum, and energy conservation equations [Eqs. (1-4)].

At the temperature of 320 K, hydrogen is transparent to the laser irradiation, and the flow will absorb no energy. If the numerical calculation starts with a 320 K initial temperature distribution, a flow with uniform 320 K temperature would result. This solution is trivial, and no plasma will be predicted. To obtain a (stable) LSP, an initial high-temperature zone around the focal point was assigned (resembling a spark ignition), where the size, position, and temperature of the "spark" were chosen by trial and error.

The computer code used in this study is similar to that of Jeng and Keefer.[13,16] Several well-defined natural and forced convective flows have been calculated using the code and agreed well with published results.[28,29] Generally, convergence of the numerical solution was achieved in 2000 iterations. The CPU time requirements were approximately 40 s for each iteration on a Masscomp-500 computer.

Results and Discussions

The same model has been used on an argon LSP using an annular laser beams by Jeng and Keefer.[13,16] The calculations were in good agreement with experimental results.[15,17] The shape, size, energy conversion efficiency, and peak temperature of the argon plasma were predicted well. Although Fowler et al.[30] reported a successful experiment in which a stable hydrogen plasma was sustained, no quantitative results, which can be used to verify the current calculations, were reported.

Figure 2 shows the configuration used for the calculation. A carbon dioxide laser, operated at 10.6 μm, was focused by an

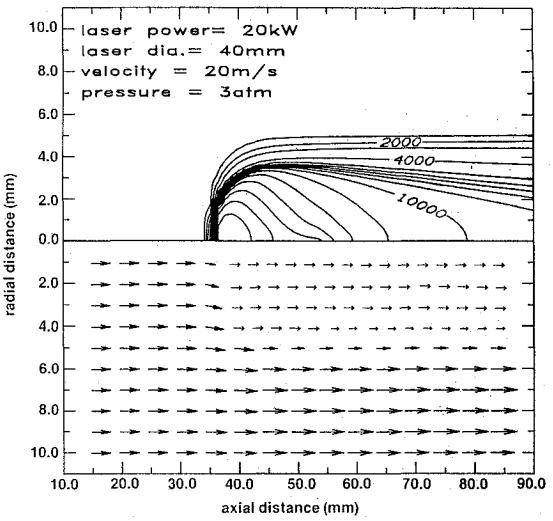

Fig. 3 Isothermal contour plot and mass flux vector plot of a calculated plasma.

8-in. focal-length lens. The peak laser intensity for this optical system is located at $x=52$ mm on the center axis. The pipe diameter was 22 mm, and the length used in the calculation was 200 mm. A uniform distribution of inlet velocity and temperature was assumed. Both wall and inlet gas temperatures were assigned the value of 320 K. Detailed description of the other boundary conditions can be found in Jeng and Keefer.[13,16] The following variation and range of flow conditions and optics were used in the parametric study: static pressure of the flow, 1–10 atm; flow inlet velocity, 5–100 m/s; laser power, 5–60 kW, and Gaussian laser beam diameter, 40–80 mm. (Gaussian laser beam diameter is defined as the e^{-2} intensity contour; the portion of the laser energy outside this diameter was neglected in the present calculations.)

Figure 3 shows the isothermal contour lines and mass flux vectors of a calculated LSP. Temperature contour lines are from 1000 to 16,000 K in 1000 K increments, and the maximum temperature of 16,804 K is located at $x=37.4$ mm, which is well upstream of the laser focal point ($x=52$ mm). The magnitude of the local mass flux, at vector origins, is proportional to the vector lengths, and the flow direction is the same as the vector directions. Figure 4 is a closeup view of the same plasma where the beam boundary is also plotted. In the bottom half of this figure, the vectors represent the velocity vectors instead of mass flux vectors. Near the center axis, upstream of the maximum temperature, the directions of energy transfer by convection and conduction are opposite, so the axial temperature gradient is large in this region. On the other hand, the temperature gradient downstream of the maximum temperature, where the mixing between inner hot and outer cold flow occurs and laser heat addition is small, is much smaller than that in the upstream region.

The temperature ratio between the core region of the LSP and the inlet is as high as 50, and the specific volume ratio can reach 150. Volumetric expansion is the dominant factor for flow acceleration. In Fig. 4, the axial velocity increases from 20 m/s at the inlet to 255 m/s in the plasma core region, but the axial mass flux (see Fig. 3) is smaller in the high-temperature region than at the inlet. Near the centerline upstream of the plasma, the axial mass flux decreases along the axial direction, so a small outward radial velocity develops (for example, at $x=35$ mm and $r=3.0$ mm in Fig. 3). The axial mass flux within the high-temperature region ($T>6000$ K) is less than one-fifth of that at the inlet, and this indicates that the constant axial mass flux assumption used by existing one-dimensional and semi-two-dimensional models[2-8] is not adequate.

Figure 5 illustrates the effect of gas inlet velocity on the LSP. As velocity increases, the plasma core moves closer to

the focal point ($x=52$ mm) where the local laser intensity is higher, because more absorbed energy is needed to balance the convection. The high-velocity plasma is smaller in diameter and has a higher maximum temperature. In the lowest-velocity ($u=5$ m/s) plasma, two local maximum temperatures are predicted, at $x=24.4$ and 52.0, respectively. Only one local maximum temperature exists, however, in the other two higher-velocity cases.

The fractional power absorption and thermal radiation loss are shown as a function of inlet velocity in Fig. 6. The LSP absorbs most of the laser irradiation, and only a very small fraction of laser power is transmitted (maximum fractional transmission is 1.7% at the lowest inlet velocity of 5 m/s). It is found that the fractional power absorption increases as the inlet velocity increases. This is because the plasma has a longer tail in the high-velocity cases, which increases the absorption path length. The fractional power lost from the plasma through thermal radiation decreases from 72% at the lowest-velocity plasma to 34% at the highest-velocity plasma. For optically thin radiation, the radiated power is proportional to the volume of the plasma size. As mentioned before, the diameter of the high-velocity plasma is smaller, which makes the plasma volume smaller, and this explains the trend of radiation power loss at different velocities, as illustrated in Fig. 6. The difference between power absorbed and power radiated represents the net power converted from the laser to the flow, and in the above test cases the radiation heat loss is the controlling factor. By increasing the inlet velocity, the net power conversion efficiency increases from 26 to 64%.

The interaction between the laser beam and the plasma is illustrated in Fig. 7. Local laser intensity distributions with no absorption, Fig. 7a, and in two low-velocity plasmas, Figs. 7b and 7c are plotted (note that the coordinate scales are different in Figs. 5 and 7). When the laser beam is focused into a nonabsorbing medium, the local laser intensity distribution in the radial direction in the absence of aberration is the same as the prefocused laser intensity distribution, and the magnitude is approximately inversely proportional to the square of the axial distance from the focal point. Since the lens used in the calculation was not perfect, a focal zone instead of a focal point was observed in Fig. 7a; however, the intensity distribution elsewhere is still close to that using a perfect lens. The local laser intensity distribution within the plasma is considerably different than the unabsorbed case. Intensity along the center axis increases as the laser beam approaches the high-temperature zone and reaches a maximum there. In the high-temperature region, strong interactions occur between the laser beam and the plasma. Initially, attenuation of laser intensity due to plasma absorption cannot be compensated for by the converging laser beam, so the intensity decreases along the axial direction and reaches a local minimum. However, beyond this point, the converging effect of the laser beam dominates the attenuation due to plasma absorption, and the local laser intensity monotonically increases to the focal zone, where the absolute maximum local intensity is located. However, more of the total laser energy passes through the focal zone in the 5 m/s inlet velocity plasma than that in the 20 m/s inlet velocity plasma, and this could explain why two local maximum temperatures were predicted in Fig. 7b.

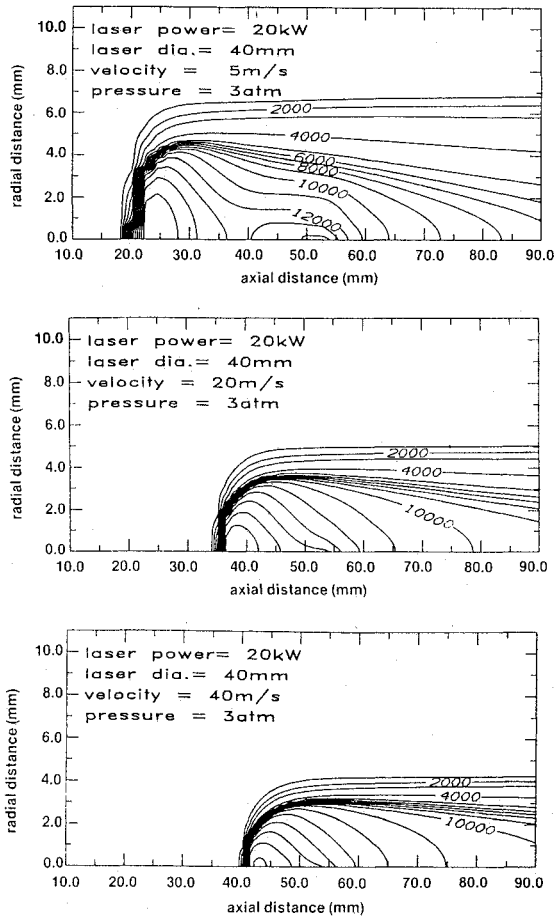

Fig. 5 Isothermal contour plots of plasmas with different inlet velocities: a) 5 m/s, b) 20 m/s, and c) 40 m/s.

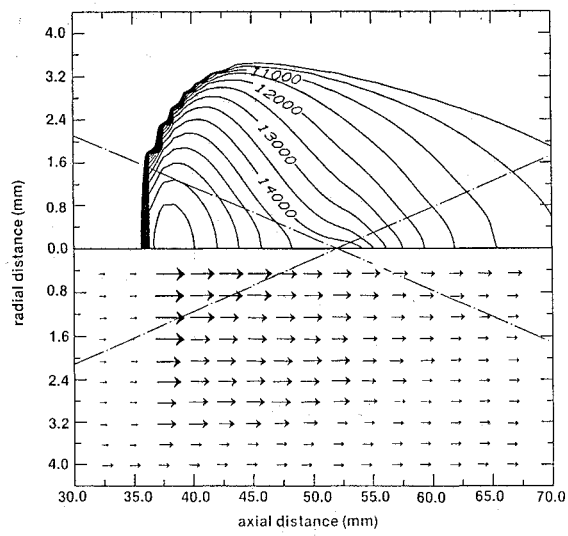

Fig. 4 Closeup view of isothermal contour plot and velocity plot of the same plasma shown in Fig. 3.

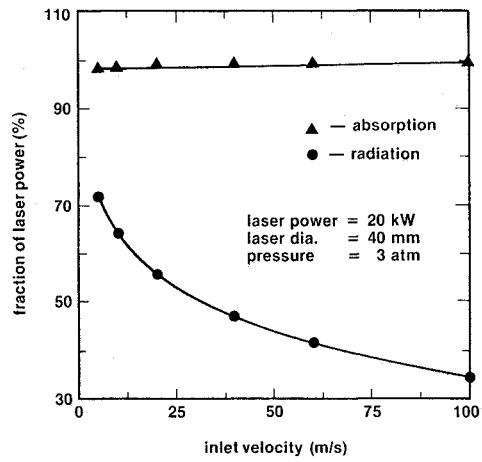

Fig. 6 Fractions of the incident laser power that are absorbed and radiated for different inlet velocities.

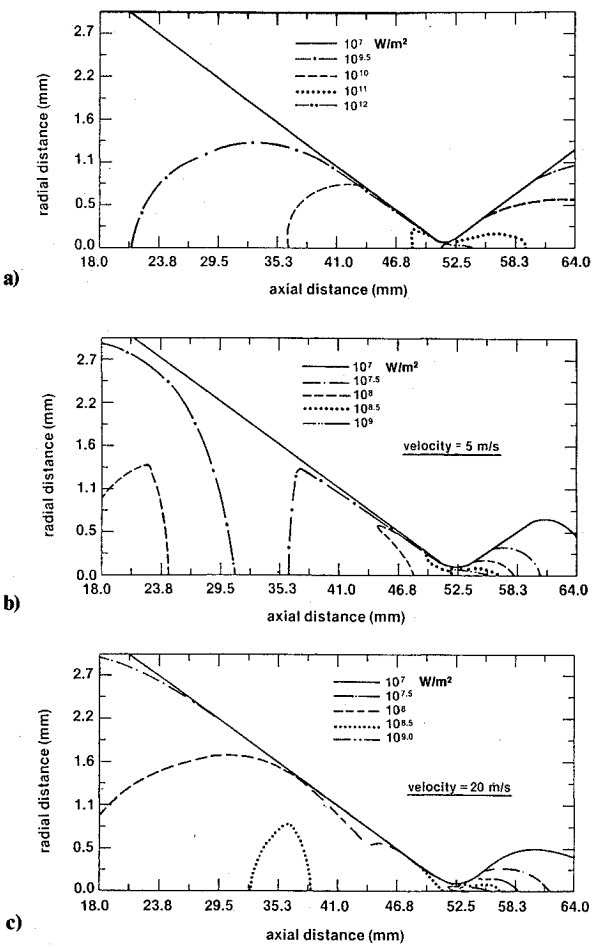

Fig. 7 Local laser intensity contour plots a) in the absence of plasma absorption, b) after plasma absorption (inlet velocity 5 m/s), and c) after plasma absorption (inlet velocity 20 m/s).

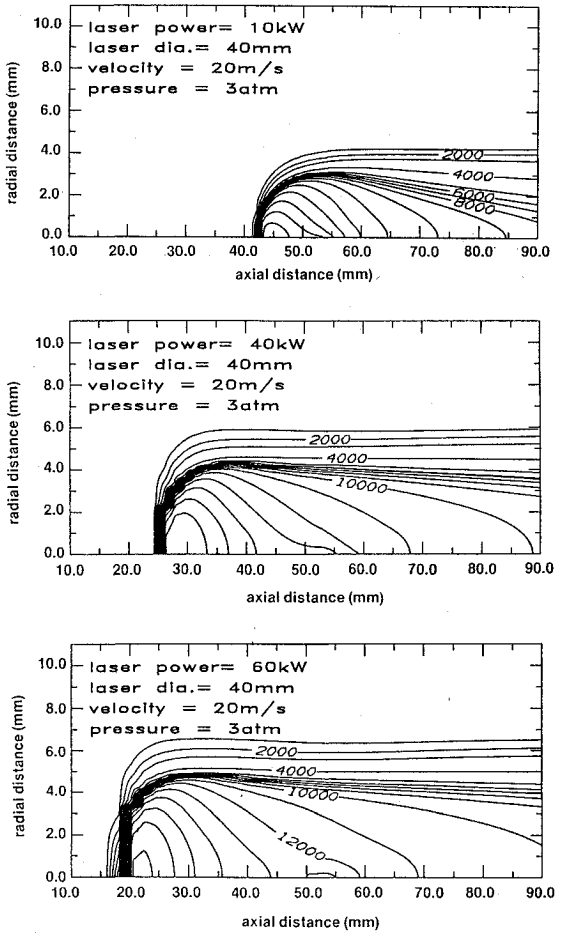

Fig. 8 Isothermal contour plots of plasmas for different incident laser powers: a) 10 kW, b) 40 kW, and c) 60 kW.

Temperature contour lines calculated using different laser powers are shown in Fig. 8. The plasma position moves further upstream as laser power increases. Higher peak temperature and larger plasma size are also predicted at higher laser power. Two local maximum temperatures are also observed in the 60 kW laser power case. Power conversion efficiency for this set of plasmas is plotted in Fig. 9. Both fractional power absorption and thermal radiation loss monotonically increase with increasing laser power, since both plasma length (which is related to the absorption path length) and diameter (which is related to the volume for optically thin radiation) are larger. Overall power converted from the laser to the flow is larger in the high laser power case, although the fractional power conversion is slightly lower.

The optical properties of the LSP are strongly dependent on the static pressure. Five calculated temperature distributions at different static pressures are shown in Fig. 10. Figures 10a-c are for constant inlet velocity, and Figs. 10b, 10d, and 10e are for constant inlet mass flow rate. The total mass flow rate is proportional to the static pressure if the inlet velocity is the same. Note that the absorption coefficient is a highly nonlinear function of static pressure. The combination of different forced convective flow (mass flow rate) and absorption coefficient makes the explanation of the LSP behavior more difficult. The laser power threshold depends on both heat addition (absorption) and heat loss (convection). For constant inlet velocity, the LSP is located further upstream as the pressure increases from 3 to 5 atm; then it moves downstream toward the focal point as the pressure continues to increase. In the outer edge or downstream of the plasma, laser heat addition is small, so the higher-pressure (higher mass flow rate)

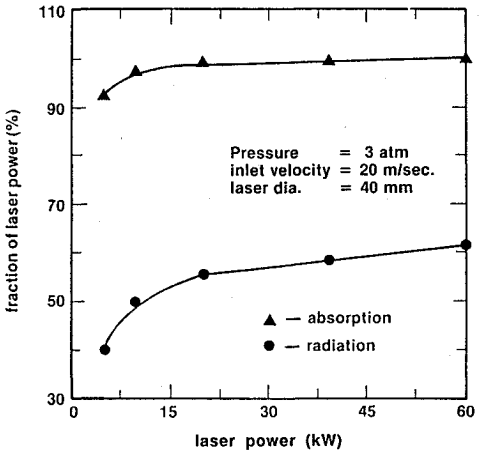

Fig. 9 Fractions of the incident laser power that are absorbed and radiated for a range of incident laser powers.

plasma has a smaller-diameter LSP. For the constant mass flow rate plasmas, the effect of forced convective flow on the LSP is similar, and the optical properties play the most important role in the results. As the pressure increases, the plasma position moves upstream. Although the plasma size is smaller at higher pressure, the difference is not substantial.

Figure 11 shows power conversion efficiencies for the above test series. At 1 atm a large amount of laser power is transmitted through the LSP. Transmitted laser power, which decreases as pressure increases, is less than 2% in the plasmas,

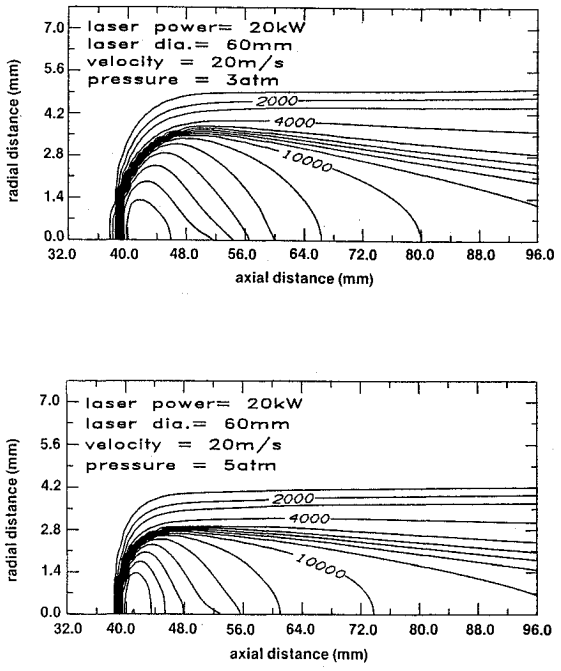

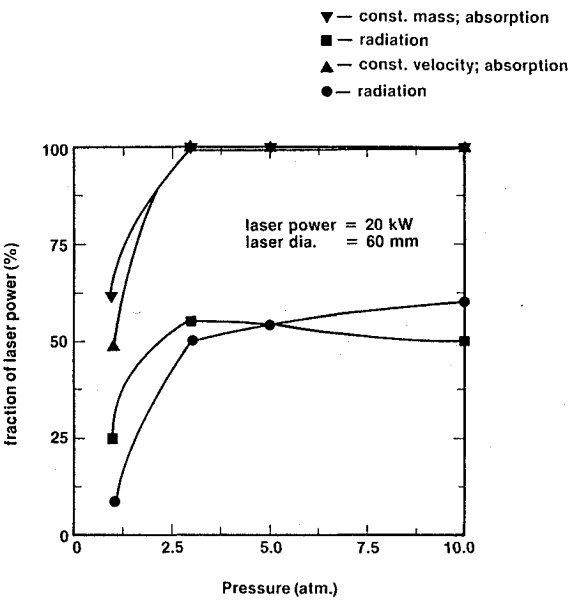

Fig. 11 Fractions of the incident laser power that are absorbed and radiated for different static pressures.

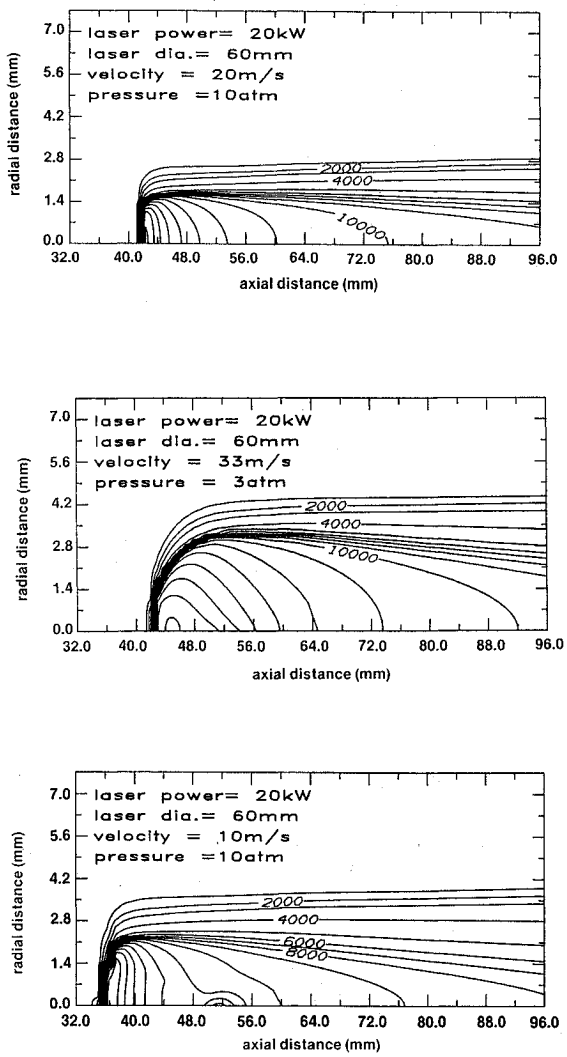

Fig. 10 Isothermal contour plots of plasmas with different static pressures.

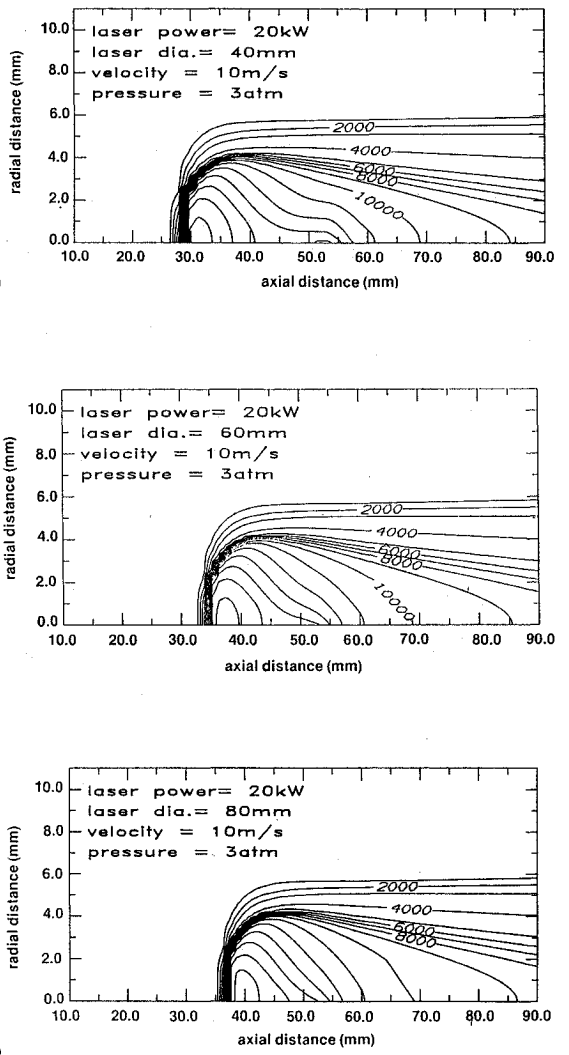

Fig. 12 Isothermal contour plots of plasmas with different incident laser beam diameters: a) 40 mm, b) 60 mm, and c) 80 mm.

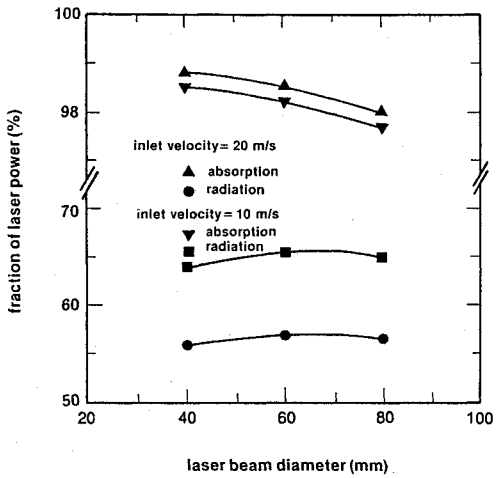

Fig. 13 Fractions of the incident laser power that are absorbed and radiated for three laser beam diameters.

with a static pressure greater than 3 atm. The thermal power radiated in the constant inlet velocity cases decreases as pressure increases, but the thermal power radiated first increases with pressure, then decreases for pressure greater than 5 atm in the constant mass flow rate cases. Generally speaking, the energy conversion efficiency has only a weak dependence on pressure in the constant mass flow rate cases. However, in the constant velocity cases, the energy conversion efficiency is greater at higher static pressure.

Effects of the optical system on the LSP were calculated using different collimated laser beam diameters with the same lens. Calculated temperature contour lines using 40, 60, and 80 mm diameters are plotted in Fig. 12. For smaller beam diameters, the plasma cores occur further upstream than for larger beam diameters. Although the plasma position is highly dependent on the laser beam diameter, the calculated peak temperature and size show only minor differences. The corresponding fractional power absorption and radiation as a function of beam diameter are plotted in Fig. 13 for two sets of inlet velocities. The smaller laser beam diameter (larger *f*/number) LSP absorbs more laser energy and has less radiation heat loss, so it has better net energy conversion efficiency.

Conclusions

Laser-sustained plasmas in a hydrogen flow have been numerically calculated using Navier-Stokes equations. The converging laser beam and realistic gas properties were also included in the model. It was found that local laser heat addition to the plasma produces a local high-pressure zone. Near the centerline upstream of the plasma, the flow is influenced by the existence of the plasma, so the radial velocity of the flow is outward; in the downstream region, the radial velocity of the flow is inward. Therefore, the axial mass flux is smallest within the core of the plasma. It is clear that a one-dimensional flow model, which uses a constant axial mass flux assumption, is not adequate for this problem.

Although two local maximum temperatures on the center axis were calculated in several cases using a Gaussian intensity distribution of the laser beam, no off-axis local temperature maximums, such as those predicted using an annular intensity distribution for an argon flow[13,16] and a Gaussian intensity distribution for a hydrogen cesium mixture flow,[10-12] were observed. The plasma was always located upstream of the focal point, and this high-temperature region absorbs most of the laser energy traveling through it. However, the outer region of the Gaussian laser beam suffers less attenuation before reaching the focal point. In some cases, a local maximum of laser intensity occurs at the focal point, although the plasma was initiated ahead of the focal point and more than one local maximum temperature existed on the center axis.

If the laser power is larger than 10 kW and the static pressure is higher than 3 atm, the LSP absorbs nearly all the laser power. In these situations, the optically thin radiation heat loss is the critical factor in the energy conversion efficiency. From the parametric study, the following trends were observed: as laser power increases, the conversion efficiency decreases, although the total laser power absorbed by the plasma increases; as flow rate increases, the conversion efficiency increases; as static pressure increases, the conversion efficiency increases for the fixed inlet velocity cases, and it remains nearly constant at fixed mass flow rate. The best conversion efficiency (65%) among the calculated cases was obtained using the highest inlet velocity, 100 m/s, with intermediate static pressure, 3 atm.

It was also found that the plasma position and size can be controlled by several parameters. In general, increasing the laser power or increasing the static pressure, which increases the absorption coefficient, tends to move the plasma upstream; increasing the flow rate, which increases the convective heat transfer, tends to push the plasma toward the focal point. The plasma diameter is highly dependent on the laser power, inlet velocity, and static pressure. Minimum plasma diameters were predicted using the combination of high inlet velocity, high static pressure, and low laser power.

Acknowledgments

This work was partially sponsored by Air Force Office of Scientific Research Grant AFOSR-83-0043. The Program Manager was Dr. Robert Vondra.

References

[1]Kantrowitz, A.R., "The Relevance of Space," *Astronautics and Aeronautics*, Vol. 9, Sept. 1971, pp. 34-35; also "Propulsion to Orbit by Ground Based Laser," *Astronautics and Aeronautics,* Vol. 19, May 1982, pp. 74-76.

[2]Raizer, Y.P., "Subsonic Propagation of a Light Spark and Threshold Conditions for the Maintenance of Plasma by Radiation," *Soviet Physics—JETP,* Vol. 31, Dec. 1970, pp. 1148-1154.

[3]Jackson, J.P. and Nielsen, P.E., "Role of Radiative Transport in the Propagation of Laser-Supported Combustion Waves," *AIAA Journal,* Vol. 12, Nov. 1974, pp. 1498-1501.

[4]Kemp, N.H. and Root, R.G., "Analytical Study of Laser-Supported Combustion Waves in Hydrogen," *Journal of Energy,* Vol. 3, Jan.-Feb. 1979, pp. 40-49.

[5]Keefer, D.R., Peters, C.E., and Crowder, H.L., "A Re-examination of the Laser Supported Combustion Wave," *AIAA Journal,* Vol. 23, Aug. 1985, pp. 1208-1212.

[6]Batteh, J.H. and Keefer, D.R., "Two-Dimensional Generalization of Rainer's Analysis for the Subsonic Propagation of Laser Sparks," *IEEE Transactions on Plasma Science,* Vol. PS-2, Sept. 1974, pp. 122-129.

[7]Keefer, D.R., Crowder, H.L., and Elkins, R., "A Two-Dimensional Model of the Hydrogen Plasma for a Laser Powered Rocket," AIAA Paper 82-0404, Jan. 1982.

[8]Glumb, R.J. and Krier, H., "Two-Dimensional Model of Laser-Sustained Plasmas in Axisymmetic Flowfields," *AIAA Journal,* Vol. 24, Aug. 1986, pp. 1331-1336.

[9]Gulati, A. and Merkle, C.L., "Absorption of Electromagnetic Radiation in an Advanced Propulsion System," *Journal of Spacecraft and Rockets,* Vol. 21, Jan.-Feb. 1984, pp. 101-107.

[10]Merkle, C.L., "Prediction of the Flowfield in Laser Propulsion Devices," *AIAA Journal,* Vol. 22, Aug. 1984, pp. 1101-1107.

[11]Merkle, C.L., Molvik, G.A., and Choi, Y.-H., "A Two-Dimensional Analysis of Laser Heat Addition in a Constant Absorptivity Gas," *AIAA Journal,* Vol. 23, July, 1985, pp. 1053-1060.

[12]Merkle, C.L., Molvik, G.A., and Shaw, E.J.-H., "Numerical Solution of Strong Radiation Gasdynamic Interactions in a Hydrogen-Seedant Mixture," AIAA Paper 85-1554, 1985.

[13]Jeng, S-M. and Keefer, D.R., "Theoretical Investigation of Laser-Sustained Argon Plasmas," *Journal of Applied Physics,* Vol. 60, Oct. 1986, pp. 2272-2279.

[14]Keefer, D.R., Crowder, H.L., and Peters, C.E., "Laser Sustained Argon Plasmas in a Forced Convection Flow," AIAA Paper 85-0388, 1985.

[15]Keefer, D.R., Welle, R.P., and Peters, C.E., "Power Absorption Processes in Laser-Sustained Argon Plasmas," AIAA Paper 85-1552, 1985.

[16]Jeng, S-M. and Keefer, D.R., "Numerical Study of Laser-Sustained Argon Plasmas in a Forced Convective Flow," AIAA Paper 86-1078, 1986.

[17]Welle, R.P., Keefer, D.R., and Peters, C.E., "Energy Conversion Efficiency in High-Flow, Laser-Sustained Argon Plasmas," AIAA Paper 86-1077, 1986.

[18]Patch, R.W., "Thermodynamic Properties and Theoretical Rocket Performance of Hydrogen to 100,000 K and 1.01325×10^8 N/m^2," NASA SP-3069, 1971.

[19]VanZandt, D.M., McCay, T.D., and Eskridge, R.H., "An Experimental Study of Laser Supported Hydrogen Plasmas," AIAA Paper 84-1572, 1984.

[20]Grier, N.T., "Calculation of Transport Properties and Heat-Transfer Parameters of Dissociating Hydrogen," NASA TN D-1406, 1962.

[21]Grier, N.T., "Calculation of Transport Properties of Ionizing Atomic Hydrogen," NASA TN D-3186, 1966.

[22]Kemp, N.H. and Root, R.G., "Analytical Study of Laser-Supported Combustion Waves in Hydrogen," *Journal of Energy*, Vol. 3, Jan.-Feb. 1979, pp. 40-49.

[23]Kemp, N.H. and Root, R.G., "Analytical Study of Laser-Supported Combustion Waves in Hydrogen," NASA CR-135349, 1977.

[24]Caledonia, G.E., Wu, P.K.S., and Pirri, A.N., "Radiant Energy Absorption Studies for Laser Propagation," NASA CR-134809, 1975.

[25]Kemp, N.H., Root, R.G., Wu, P.K.S., Caledonia, C.E., and Pirri, A.N., "Laser-Heated Rocket Studies," NASA CR-136127, 1977.

[26]Patankar, S.V., *Numerical Heat Transfer and Fluid Flow*, Hemisphere, Washington, DC, 1980.

[27]Gosman, A.D., Pun, W.M., Ruchal, A.K., Spalding, D.B., and Wolfshtein, R., *Heat and Mass Transfer in Recirculating Flows*, Academic Press, Orlando, FL, 1969.

[28]Newell, M.E. and Schmidt, F.W. "Heat Transfer by Laminar Natural Convection Within Rectangular Enclosures," *Journal of Heat Transfer*, Vol. 92, Feb. 1970, pp. 159-165.

[29]Armaly, B.F., Durst, F., Pereira, J.C.F., and Schonung, B., "Experimental and Theoretical Investigation of Backward-Facing Step Flow," *Journal of Fluid Mechanics*, Vol. 127, Feb. 1983, pp. 473-496.

[30]Fowler, M.C., Newman, L.A., and Smith, D.C., "Beamed Energy Coupling Studies—Final Report," AFRPL-TR-79-51, Jan. 1980.